2D and 3D modeling and optimization for the design of a fast hydrodynamic focusing microfluidic mixer

Benjamin Ivorra, Juana L. Redondo, Juan G. Santiago,
Pilar M. Ortigosa and Angel M. Ramos

Mayo-2012

2D and 3D modeling and optimization for the design of a fast hydrodynamic focusing microfluidic mixer.

Benjamin Ivorra (1), Juana L. Redondo (2), Juan G. Santiago (3),
Pilar M. Ortigosa (4) and Angel M. Ramos (1)

(1) Dept. de Matemática Aplicada,
Universidad Complutense de Madrid,
Plaza de Ciencias, 3, 28040 Madrid, Spain.
(2) Dept. de Arquitectura y Tecnología de Computadores,
Universidad de Granada, Periodista Daniel Saucedo Aranda,
18071 Granada, Spain
(3) Mechanical Engineering Dept., Stanford University,
440 Escondido Mall, Stanford, CA. 94305-3030, U.S.A.
(4) Dept. de Arquitectura de Computadores y Electrónica,
Universidad de Almeria, ceiA3, Ctra. Sacramento,
La Cañada de San Urbano, 04120 Almería, Spain.

April 26, 2012

Abstract

In this paper, we are interested in the design of a microfluidic mixer based on hydrodynamic focusing which is used to initiate the folding process (i.e., changes of the molecular structure) of a protein by diluting a protein solution to decrease its denaturant concentration to a given value in a short time interval we refer to as mixing time. Our objective is to optimize this mixer by choosing suitable shape and flow conditions in order to minimize its mixing time. To this end, we first introduce a numerical model that enables computation of the mixing time of a considered mixer. To reduce the computational time needed to solve our design problem, this model is implemented in both full three-dimensional (3D) and simplified two-dimensional (2D) versions; and we analyze the ability of the 2D model to approximate the mixing time predicted by the 3D model. Then, we define a mixer optimization problem and solve it using a hybrid global optimization algorithm. We verify the robustness of the optimized result by performing a sensitivity analysis of its parameters. We achieve a design with a predicted mixing time of 0.10 μs, approximately one order of magnitude faster than previous mixers.

1   Introduction

Proteins are composed of chains of amino acids which can assume complex three-dimensional (3D) structures. Protein folding refers to the processes by which inactive proteins (unfolded chains of amino acids) acquire the 3D shapes (called folded) enabling them to perform a wide range of biological functions [1, 2]. The applications of protein folding in research and industry are numerous, including: drug discovery, DNA sequencing and amplification, molecular diagnostics and food engineering (see, for instance, [3, 4]). Protein folding can be initiated, for instance, by using photochemical initiation [5], changes in temperature and/or pressure [3, 6] or changes in chemical potential (such as concentration of a chemical species) [7]. All these techniques provide perturbations of a protein conformational equilibrium [1], necessary to begin folding. The folding techniques based on rapid changes in concentration of chemical species are among the most versatile [8].

The original concept of a micromixer based on diffusion from (or to) a hydrodynamically focused stream was first proposed by Brody et al. [9]. As shown in Figure 1, this kind of mixer is composed of three inlet channels and a common outlet channel. It is symmetric with respect to its center channel. In the center inlet channel a mixture of unfolded proteins and a chemical denaturant is injected, whereas in the two side inlet channels a background buffer is introduced [10]. The objective is to rapidly decrease the denaturant concentration in order to initiate protein folding in the outlet channel [10]. Since the publication of Brody et al., there have been significant advances in this field. As summarized by Hertzog et al. [11, 12] and Yao and Bakajin [13], these include reduction in consumption rate of reactants, methods of detection, fabrication and, the most important improvement, reduction of the so called mixing time (i.e., time needed to reach a required denatruant concentration threshold). Indeed, the mixing time determines the temporal resolution by which protein folding kinetics can be analyzed. For example, while the original mixer of Brody et al. [9] showed mixing times greater than 10 μs (given the mixing measures used here), Hertzog et al. [11] obtained mixing times of 1.2 μs. Furthermore, Hertzog et al. [11, 12] and Yao and Bakajin [13] pointed out the importance of 3D flow effects and flow inertia in the designs of these mixers but, due to computational limitations, they considered only 2D flow models.

In this article, we present both 2D and 3D modeling for the optimization of the shape and flow conditions of a particular hydrodynamic focused microfluidic mixer. Our objective is to improve a specified mixing time of this device taking into account that, currently, the best mixer designs exhibit

mixing times of approximately 1.0 μs [11, 13]. To do so, we first introduce a mathematical model which computes mixing time for a given mixer geometry and injection velocities. We develop 2D and 3D versions of this model in order to study the ability of the 2D model to approximate key results of the 3D model. Then, we define the considered optimization problem based on the 2D model. We note that our 2D model is more complex than the one presented in [11, 14], as it includes new variables such as both the angle of inlet channels near the intersection and inlet flow velocities. This problem is solved by considering a hybrid global optimization method which is itself an improvement of a technique previously used for designing microfluidic mixers [14]. Finally, using the 3D model, we analyze the proposed optimized mixer to check the validity of the approach to designing based on the 2D model and also its robustness to parameters perturbations.

The paper is organized as follows: Section 2 introduces the 2D and 3D models used to compute the mixing times. Section 3 describes the numerical experiments carried out during this work: a comparison of the models, the optimization process and sensitivity analysis. Lastly, Section 4 presents our optimized design results and compare these to published studies [11, 14].

2   Microfluidic mixer modeling

Here, we detail the mathematical models used to perform both optimization process and sensitivity analysis. More precisely, in Subsection 2.1, we define the 2D and 3D models which describe the denaturant concentration distribution of the mixer. In Subsection 2.2, we introduce the mixer parameterization determining its shape and flow conditions. Finally, in Subsection 2.3, we show how mixing time is computed.

Note that the type of model and numerical approach used here to predict mixing times for given geometry and flow conditions has been validated experimentally in previous studies, including [11, 12, 13].

2.1   Mathematical Model

We consider the microfluididic hydrodynamic focusing mixer introduced in Section 1.

Let Ω_{3D} be the domain defined by the mixer shape in 3D. A typical representation of Ω_{3D} is depicted in Figure 1. The mixer geometry has two symmetry planes that can be used to reduce the simulation domain. Therefore, it is only necessary to study a quarter of the mixer, denoted by $\Omega_{3D,s}$ and represented in dark gray in Figure 1. Furthermore, $\Omega_{3D,s}$ can be approximated considering a 2D projection, as suggested in other works [11, 15, 16]. A representation of this projection, denoted by $\Omega_{2D,s}$, is shown in Figure 2.
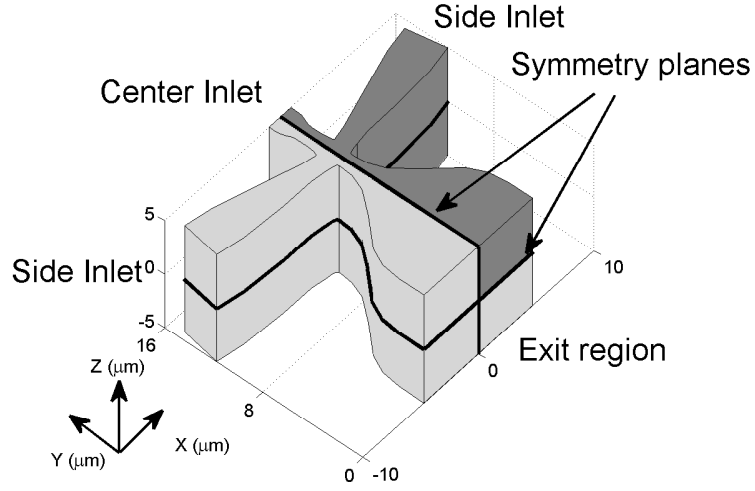
Figure 1: Typical domain representation of the microfluidic mixer geometry considering the 3D model: in dark gray we represent the domain $\Omega_{3D,s}$ used for numerical simulations. The geometry's symmetry planes are highlighted and labeled.
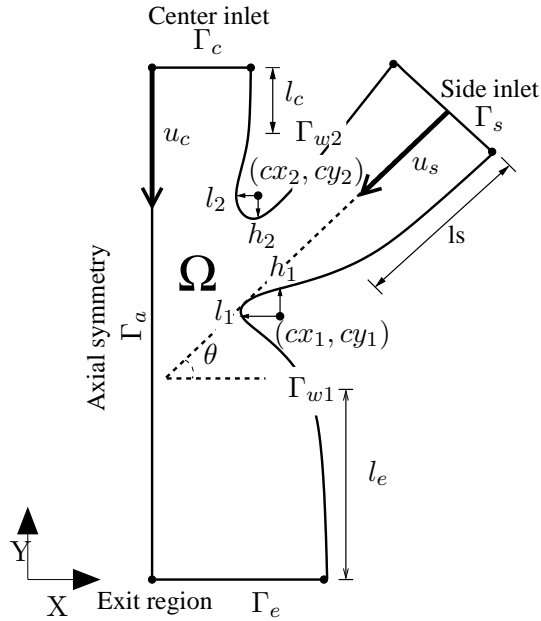

Figure 2: Typical representation of the domain $\Omega_{2D,s}$ and parameterization of the microfluidic mixer considered for the optimization process.

For the sake of simplicity, the system of coupled equations introduced below and describing the distribution of the denaturant concentration in the

mixer is defined only for the 2D case. The 3D model can be obtained easily by extruding the domain $\Omega_{2D,s}$, the equations and the boundary conditions with the considered mixer depth (i.e, mixer length in the Z-axis) [17].

In order to simplify the notations, we introduce $\Omega = \Omega_{2D,s}$. In the boundary of Ω, denoted by Γ, we define: Γ_c the boundary representing the center inlet; Γ_s the boundary representing the side inlet; Γ_e the boundary representing the outlet; Γ_{w1} the boundary representing the wall defining the lower corner; Γ_{w2} the boundary representing the wall defining the upper corner; Γ_a the boundary representing the Y-axis symmetry. A geometrical representation of these boundaries is given in Figure 2.

We assume the mixer liquid flow is incompressible [12]. Thus, the concentration distribution of the denaturant is described by using the incompressible Navier-Stokes equations coupled with the convective diffusion equation [18]. Since we do not need the behavior of the device during its transient set up, only steady configurations are considered. More precisely, we approximate the flow velocity and the denaturant concentration distribution by considering the solution of the following system of equations [11, 12]:

$$
\begin{cases}
-\nabla \cdot (\eta(\nabla \mathbf{u} + (\nabla \mathbf{u})^\top) - p) + \rho(\mathbf{u} \cdot \nabla)\mathbf{u} = 0 & \text{in } \Omega, \\
\nabla \cdot \mathbf{u} = 0 & \text{in } \Omega, \\
\nabla \cdot (-D\nabla c) + \mathbf{u} \cdot \nabla c = 0 & \text{in } \Omega,
\end{cases}
\tag{1}
$$

where c is the denaturant normalized concentration distribution, $\mathbf{u}$ is the flow velocity vector (m s^{-1}), p is the pressure field (Pa), D is the diffusion coefficient of the denaturant in the background buffer (m^2 s^{-1}), η is the denaturant dynamic viscosity (kg m^{-1} s^{-1}) and ρ is the denaturant density (kg m^{-3}).

System (1) is completed by the following boundary conditions:

For the flow velocity $\mathbf{u}$:

$$
\begin{cases}
\mathbf{u} = 0 & \text{on } \Gamma_{w1} \cup \Gamma_{w2}, \\
\mathbf{u} = -u_s \text{para}_1 \mathbf{n} & \text{on } \Gamma_s, \\
\mathbf{u} = -u_c \text{para}_2 \mathbf{n} & \text{on } \Gamma_c, \\
p = 0 \text{ and } (\eta(\nabla \mathbf{u} + (\nabla \mathbf{u})^\top))\mathbf{n} = 0 & \text{on } \Gamma_e, \\
\mathbf{n} \cdot \mathbf{u} = 0 \text{ and } \mathbf{t} \cdot (\eta(\nabla \mathbf{u} + (\nabla \mathbf{u})^\top) - p)\mathbf{n} = 0 & \text{on } \Gamma_a,
\end{cases}
\tag{2}
$$

where u_s and u_c are the maximum side and center channel injection velocities (m s^{-1}), respectively; para$_1$ and para$_2$ are the laminar flow profiles (parabolas for the 2D case and paraboloids of revolution for the 3D case) equal to 0 in the inlet border and unity in the inlet center [18]; and $(\mathbf{t}, \mathbf{n})$ is the local orthonormal reference frame along the boundary.

For the concentration c:

$$
\begin{cases}
\mathbf{n} \cdot (-D\nabla c + c\mathbf{u}) = -c_0 \mathbf{u} & \text{on } \Gamma_c, \\
c = 0 & \text{on } \Gamma_s, \\
\mathbf{n} \cdot (-D\nabla c) = 0 & \text{on } \Gamma_e, \\
\mathbf{n} \cdot (-D\nabla c + c\mathbf{u}) = 0 & \text{on } \Gamma_{w1} \cup \Gamma_{w2} \cup \Gamma_a,
\end{cases}
\tag{3}
$$

5

where $c_0 = 1$ is the initial denaturant normalized concentration in the center inlet. We note that the first equality in (3) corresponds to the inward denaturant flux in the center inlet channel and the third equality to the convective flux leaving the outlet channel.

2.2 Mixer parameterization

We first introduce the parameterization used to describe the mixer shape Γ. We consider several constraints related to the mixer microfabrication process [12, 19, 20]: (i) the desired structural strength of the device requires a maximum angle θ at the intersection channels of $\pi/3$; (ii) the depth of the mixer is set to 10 μm to avoid clogging issues, to account for the resolution limits of confocal microscopy (used to measure experimentally the mixing time) and to mitigate the effects of the top and bottom walls on mixing dynamics; (iii) the width of the side and center channel nozzles (i.e., the length of Γ_c and twice the length of Γ_s, respectively) are set to 2 μm and 3 μm, respectively; and (iv) the mixer maximum length (i.e, length in the X-axis) and the mixer maximum height (i.e, length in the Y-axis) are set to 24 and 30 μm, respectively.

Taking these limitations into account, the mixer shape is described by rational Bézier curves and two ellipsoids. The latter are denoted as ellipsoids 1 and 2, where part of the ellipsoid 1 joins, in Γ_{w1}, the outlet and side channels, and part of the ellipsoid 2 joins, in Γ_{w2}, the center and side channels. These curves are determined by the following parameters (see Figure 2 for their geometrical representation), suitably bounded to avoid non-admissible shapes (i.e., shape with intersected curves): the angle $\theta \in [0, \pi/3]$ between Γ_c and the direction normal to Γ_s; the length of the center inlet channel $l_c \in [2.5 \ \mu\text{m}, 5 \ \mu\text{m}]$; the length of the side inlet channel $l_s \in [1 \ \mu\text{m}, 9 \ \mu\text{m}]$; the length of the outlet channel $l_e \in [0.1 \ \mu\text{m}, 20 \ \mu\text{m}]$; the coordinates of the center of the ellipsoid i, with $i = 1, 2$, (cx_i, cy_i) , where $cx_1 \in [0.8 \ \mu\text{m}, 3 \ \mu\text{m}]$, $cy_1 \in [l_e \ \mu\text{m}, l_e + 2 \ \mu\text{m}]$, $cx_2 \in [0.8 \ \mu\text{m}, 0.9 \ \mu\text{m}]$ and $cy_2 \in [cy_1 + 1 \ \mu\text{m}, cy_1 + 3) \ \mu\text{m}]$; the radius l_i in the X-axis of the ellipsoid i, with $i = 1, 2$, satisfies $l_i \in [0 \ \mu\text{m}, (cx_i - 0.5) \ \mu\text{m}]$; the radius h_i in the Y-axis of the ellipsoid i, with $i = 1, 2$, h_i, satisfies $h_1 \in [0 \ \mu\text{m}, (cy_2 - cy_1 - 1) \ \mu\text{m}]$ and $h_2 \in [0 \ \mu\text{m}, (cy_2 - cy_1 - 1 - h_1) \ \mu\text{m}]$.

In addition to those parameters, we also consider the maximum injection velocities u_s and u_c as design variables. Furthermore, in order to maintain laminar flow and to avoid secondary flows in the outlet channel, such as Dean vortices [21, 22], we constrained the typical flow Reynolds Re to less than 15 [13, 18, 20]. We define $Re = \rho u_s L / \eta$, where $L = 3 \ \mu$m is the side channel nozzle width. This implies that $u_s \leq \eta Re / \rho L$ m s^{-1}. Moreover, in practice, u_c should be at least 10 times lower than u_s to ensure a good mixing between fluids [11]. Therefore, we impose that $u_s \in [0, \eta Re / \rho L]$ m s^{-1} and $u_c = p \times u_s$, where $p \in [0.001, 0.1]$.

Thus, the set of parameters defining a particular mixer design is denoted by

$$\phi = \{u_s, p, \theta, l_c, l_s, l_e, cx_1, cy_1, l_1, h_1, cx_2, cy_2, l_2, h_2\} \in \Phi,$$

where $\Phi = \Pi_{i=1}^{14}[\underline{\Phi}(i), \overline{\Phi}(i)] \subset \mathbb{R}^{14}$ is the admissible space; and $\underline{\Phi}(i) \in \mathbb{R}$ and $\overline{\Phi}(i) \in \mathbb{R}$ are the upper and lower constraint values of the i-th parameter in ϕ described previously, respectively.

2.3   Mixing time

In this work, the mixing time is defined as the time required to change the denaturant normalized concentration of a typical Lagrangian stream fluid particle situated in the symmetry streamline at depth $z = 0$ μm (halfway between the top and the bottom walls) from $\alpha \in [0, 1]$ to $\omega \in [0, 1]$ [11, 12, 13, 14]. We remark that the choice of α and ω has a great impact on the mixing time. This choice is influenced by several factors, such as the type of denaturant [10]. For example, α is set by the minimum denaturant concentration for which we can be confident the protein stays unfolded, while ω is set by the maximum concentration for which we can be confident it folds.

Thus, the mixing time of a particular mixer described by the parameters $\phi \in \Phi$, and denoted by J_{2D} for the 2D case and J_{3D} for the 3D case, is computed by:

$$J_{iD}(\phi) = \int_{c_\omega^\phi}^{c_\alpha^\phi} \frac{\mathrm{d}y}{\mathbf{u}^\phi(y)}, \tag{4}$$

where i is the dimension of the problem (i.e., $i = 2$ or 3); $\mathbf{u}^\phi$ and c^ϕ denote the solution of System (1)-(3), in its iD version, when considering the mixer defined by ϕ; and c_α^ϕ and c_ω^ϕ denote, for the 2D case (3D case, respectively), the points situated along the symmetry streamline (the streamline defined by the intersection of the two symmetry planes $z = 0$ μm and $x = 0$ μm, respectively) where the denaturant normalized concentration is α and ω.

3   Numerical Experiments

In this Section, we first introduce our numerical implementation of the 2D and 3D models. Then, we describe the numerical experiments accomplished to compare both models, to optimize the mixer and to analyze the validity and robustness of the optimized result.

3.1   Numerical implementation of the model

The numerical versions of both 2D and 3D models, presented in Section 2, are implemented by coupling Matlab scripts (www.mathworks.com) with COMSOL Multiphysics 3.5a models (www.comsol.com). More precisely, to

compute a numerical solution of System (1)-(3), we consider a Finite Element Method (FEM) with Lagrange P2-P1 elements to stabilize the pressure and to satisfy the Ladyzhenskaya, Babouska and Brezzi stability condition. The 2nd-order Lagrange elements model the velocity and concentration components, while linear elements represent the pressure. The Navier-Stokes equations are solved using Galerking Least Square streamline and crosswind diffusion methods in order to prevent numerical oscillations. The convective diffusion equation is solved by considering an upwind scheme. We use a Direct Damped Newton method to solve the corresponding linear systems. Finally the mixing time, defined by Equation (4), is estimated by considering the solutions of previous FEM model and a trapezoidal approximation of the integral. A complete description of those techniques can be found in [23].

The computational experiments are carried out in a 2.8GHz Intel i7-930 64-bit computer with 12GB of RAM. For the 2D simulations described in Sections 3.2 and 3.3, we use a Delaunay mesh with around 6000 elements. In that case, a single evaluation for J_{2D} requires about 35 s. The 3D simulations, conducted during Sections 3.2 and 3.4, are performed with a Delaunay mesh containing 13000 elements. Each evaluation of J_{3D} takes approximatively 30 min.

3.2 Comparison between 2D and 3D models

First, a comprehensive computational study is carried out to determine if both 2D and 3D models yield similar mixing times when they are evaluated with the same set of parameters. Indeed, if both models have a similar behavior, the computational effort for solving the optimization problem presented in Section 3.3 can be reduced by using the 2D model instead of the 3D one (see Section 3.1).

Let $\{\phi_i\}_{i=1}^{100}$ be a set of 100 mixers randomly generated in Φ by considering a uniform distribution. For each one of them, we evaluate: the concentration distribution $c_{2D}(\phi_i)(x,y)$, the velocity field $\mathbf{u_{2D}}(\phi_i)(x,y)$ and the mixing time $J_{2D}(\phi_i)$ for the 2D model; the concentration distribution $c_{3D}(\phi_i)(x,y,0)$ and the velocity field $\mathbf{u_{3D}}(\phi_i)(x,y,0)$ in the plane $z = 0$ μm, and the mixing time $J_{3D}(\phi_i)$ for the 3D model. Then, we compute the relative difference, in percentage, between the solutions obtained by the 2D and 3D models as following:

$$100\frac{|J_{2D}(\phi_i) - J_{3D}(\phi_i)|}{J_{2D}(\phi_i)}, \tag{5}$$

$$\frac{100}{\int_\Omega \mathrm{d}x\mathrm{d}y} \int_\Omega \frac{|c_{2D}(\phi_i)(x,y) - c_{3D}(\phi_i)(x,y,0)|}{|c_{2D}(\phi_i)(x,y)|}\mathrm{d}x\mathrm{d}y, \tag{6}$$

8

$$\frac{100}{\int_\Omega \mathrm{d}x\mathrm{d}y} \int_\Omega \frac{\|\mathbf{u_{2D}}(\phi_i)(x,y) - \mathbf{u_{3D}}(\phi_i)(x,y,0)\|_2}{\|\mathbf{u_{2D}}(\phi_i)(x,y)\|_2} \mathrm{d}x\mathrm{d}y. \tag{7}$$

Additionally, for each of those quantities, we calculate the mean, minimum and maximum values regarding the 100 generated mixers.

Finally, we want to know if the 2D model preserve the same order of mixing time between two particular mixers as the 3D model. To do so, we sort the previous 100 mixers by their J_{2D} value, and analyze in which proportion the order is maintained regarding J_{3D}.

3.3 Design problem and considered global optimization algorithm

The objective is to design a microfluidic mixer described by parameters $\phi \in \Phi$, where $\Phi \subset \mathrm{I\!R}^N$ and $N = 14$, that minimizes the mixing time function J_{2D} defined in Section 2.3. Thus, the associated optimization problem can be written as:

$$\min_{\phi \in \Phi} J_{2D}(\phi). \tag{8}$$

In order to solve Problem (8), we use the particular MATLAB implementation of a global optimization algorithm included in the software called *Global Optimization Platform* and freely available at

http://www.mat.ucm.es/momat/software.html

This algorithm is a meta-heuristic global optimization method [24, 25, 26] based on a hybridization between a genetic algorithm (GA) [27] (which approximates the solution of (8)) with a multi-layer secant algorithm (MSA) [28, 29] (which provides suitable initial populations for the GA). In the following, both GA and MSA methods are described in more details. A complete validation of these algorithms on various industrial problems can be found in [14, 29, 30, 31, 32, 33].

Broadly speaking, GAs are search techniques which try to solve problems like (8) through a stochastic process based on an analogy with the Darwinian evolution of species [27]. The GAs have many advantages as for example: they do not require sensitivity computation, they can solve complex optimization problems (e.g., with high dimensional search space or function with various with local minima), and they are intrinsically parallel. However, they also have some important drawbacks, as they exhibit slower convergence and lower accuracy than other method, such as gradient algorithms. Next, we describe the GA considered during this work:

- **Step 1- Inputs:** User must define four parameters: $N_p \in \mathrm{I\!N}$, $N_g \in \mathrm{I\!N}$, $p_m \in [0, 1]$ and $p_c \in [0, 1]$. The meaning of those parameters is clarified later in the following steps. In addition, a first set, called 'initial

population' and denoted by $X^0 = \{x_j^0 \in \Phi, j = 1, ..., N_p\}$, of N_p points (called 'individuals') in Φ is also provided by user.

- **Step 2- Generating new populations:** Starting from X^0, we recursively create N_g new populations by applying four stochastic processes: 'selection', 'crossover', 'mutation' and 'elitism', which are described in Steps 3.1, 3.2, 3.3 and 3.4, respectively.

  More precisely, let $X^i = \{x_j^i \in \Phi, j = 1, ..., N_p\}$, with $i = 1, ..., N_g - 1$, denotes the population at iteration i. Then, using the (N_p, N)-real valued matrix:

  $$X^i = \begin{bmatrix} x_1^i \\ \vdots \\ x_{N_p}^i \end{bmatrix} = \begin{bmatrix} x_1^i(1) & \dots & x_1^i(N) \\ \vdots & \ddots & \vdots \\ x_{N_p}^i(1) & \dots & x_{N_p}^i(N) \end{bmatrix},$$

  with $x_j^i = (x_j^i(1), ..., x_j^i(N)) \in \Phi$, X^{i+1} is obtained by considering:

  $$X^{i+1} = (I_N - \mathcal{E}^i)(\mathcal{C}^i \mathcal{S}^i X^i + \mathcal{M}^i) + \mathcal{E}^i X^i,$$

  where matrices $\mathcal{S}^i$, $\mathcal{C}^i$, $\mathcal{M}^i$, $\mathcal{E}^i$ and I_N are described as follows.

  - **Step 2.1- Selection:** We randomly select N_p individuals from X^i with eventual repetitions. Each individual $x_j^i \in X^i$, with $j = 1, ..., N_p$, has a probability to be selected during this process which is given by $J_{2D}^{-1}(x_j^i) / \sum_{k=1}^{N_p} J_{2D}^{-1}(x_k^i)$. This step can be summarized as

    $$X^{i+1,1} = \mathcal{S}^i X^i,$$

    where $\mathcal{S}^i$ is a (N_p, N_p)-matrix with $\mathcal{S}_{j,k}^i = 1$ if the k-th individual of X^i is the j-th selected individual and $\mathcal{S}_{j,k}^i = 0$ otherwise.

  - **Step 2.2- Crossover:** For each pair of consecutive individuals (rows) $2j - 1$ and $2j$ in $X^{i+1,1}$, with $1 \le j \le \text{floor}(N_p/2)$ (where $\text{floor}(X)$ is the nearest integer lower or equal than X), we determine, with a probability p_c, if those rows exchange data or if they are directly copied into an intermediate population denoted by $X^{i+1,2}$. Mathematically, this step can be written as:

    $$X^{i+1,2} = \mathcal{C}^i X^{i+1,1},$$

    where $\mathcal{C}^i$ is a real-valued (N_p, N_p)-matrix. The coefficients of the $(2j - 1)$-th and $2j$-th rows of $\mathcal{C}^i$, with $1 \le j \le \text{floor}(N_p/2)$, are given by:

    $$\mathcal{C}_{2j-1,2j-1}^i = \lambda_1, \ \ \mathcal{C}_{2j-1,2j}^i = 1 - \lambda_1, \ \ \mathcal{C}_{2j,2j}^i = \lambda_2, \ \ \mathcal{C}_{2j,2j-1}^i = 1 - \lambda_2$$

    where $\lambda_1 = \lambda_2 = 1$, with a probability $1 - p_c$, or λ_1 and λ_2 are randomly chosen in $]0, 1[$, considering a uniform distribution, in

other case. Other coefficients of $\mathcal{C}^i$ are set to 0. If N_p is odd then we also set $\mathcal{C}^i_{N_p,N_p} = 1$ and then the N_p-th row of $X^{i+1,1}$ is directly copied in $X^{i+1,2}$.

– **Step 2.3- Mutation:** We decide, with a probability p_m, if each row of $X^{i+1,2}$ is randomly perturbed or not. This step is defined by:

$$X^{i+1,3} = X^{i+1,2} + \mathcal{M}^i,$$

where $\mathcal{M}^i$ is a real-valued (N_p, N)-matrix where the j-th row, $j = 1, ..., N_p$, is equal to 0, with a probability 1-p_m, or a random vector $m_j \in \mathbb{R}^N$, generated considering a uniform distribution in the subset of $\mathbb{R}^N$ such that $x_j^{i+1,2} + m_j \in \Phi$, otherwise.

– **Step 2.4- Elitism:** Let x_b^i, where $b \in 1, ..., N_p$, be the individual in X^i with the lowest value of J_{2D} (or, if there exists various, one of those individuals selected randomly). If x_b^i has a lower J_{2D} value than all the individuals in $X^{i+1,3}$, it is directly copied at the b-th row of X^{i+1}. This step can be formalized as:

$$X^{i+1} = (I_N - \mathcal{E}^i)(X^{i+1,3}) + \mathcal{E}^i X^i,$$

where I_N is the identity matrix of size N and $\mathcal{E}^i$ is a real-valued (N_p, N_p)-matrix such that $\mathcal{E}^i(b,b) = 1$ if x_b^i has a lower J_{2D} value than all the individuals in $X^{i+1,3}$ and 0 otherwise, $\mathcal{E}^i = 0$ elsewhere.

• **Step 3- Output:** After N_g iterations, the GA stops and returns an output solution denoted by

$$GAO(X^0, N_p, N_g, p_m, p_c) = \text{argmin}\{J_{2D}(x_j^i)/$$
$$x_j^i \text{ is the } j\text{-th row of } X^i, i = 1, ..., N_g, j = 1, ..., N_p).$$

In order to improve the precision and the computational time of the GA previously described, we consider the MSA described next:

• **Step 1- Inputs:** The user define the following parameters: $l_{\max} \in \mathbb{N}, N_p \in \mathbb{N}, N_g \in \mathbb{N}, p_m \in [0, 1]$ and $p_c \in [0, 1]$.

• **Step 2- Initial population:** $X_1^0 = \{x_{1,j}^0 \in \Phi, j = 1, ..., N_p\}$ is randomly generated, considering a uniform distribution.

• **Step 3- Main loop:** For l from 1 to $l_{\max}$:

– **Step 3.1-** We compute $o_l = GAO(X_l^0, N_p, N_g, p_m, p_c)$.

– **Step 3.2-** We build $X_{l+1}^0 = \{x_{l+1,j}^0 \in \Phi, j = 1, ..., N_p\}$ as following:

$\forall j \in \{1, ..., N_p\}$, if $J_{2D}(o_l) = J_{2D}(x_{l,j}^0)$ we set

$$x_{l+1,j}^0 = x_{l,j}^0,$$

else we set

$$x_{l+1,j}^0 = \text{proj}_\Phi(x_{l,j}^0 - J_{2D}(o_l)\frac{o_l - x_{l,j}^0}{J_{2D}(o_l) - J_{2D}(x_{l,j}^0)}),$$

where $\text{proj}_\Phi : \mathbb{R}^N \to \Phi$ is the projection function such that $\text{proj}_\Phi(x)(i) = \min(\max(\ x(i), \underline{\Phi}(i)), \overline{\Phi}(i))$, with $i = 1, ..., N$.

- **Step 4- Output:** The algorithm returns the following output:

$$MSAO(l_{\max}, N_p, N_g, p_m, p_c) = \text{argmin}\{J_{2D}(o_l)/l = 1, ..., l_{\max}\}.$$

The numerical experiments presented in [30, 33] suggest that considering the previous MSA instead of GA alone reduces the computational time needed to solve optimization problems.

We denote by

$$\phi_o = MSAO(l_{\max}, N_p, N_g, p_m, p_c)$$

the result obtained at then end of the optimization process.

3.4 Analysis of the optimized result

Firstly, we want to check the improvements obtained by our optimized mixer. Additionally, we want to study the behavior of ϕ_o when considering the 3D model. Indeed, some important effects cannot be appreciated with the 2D model, as for example, the impact of upper and lower mixer walls on the velocity field or possible effects of certain secondary flows. To this aim, we analyze the mixing time, the shape, the final concentration and the velocity field of ϕ_o by considering both 2D and 3D models and compare them to other results found in literature [11, 13, 14].

Secondly, we want to perform a simple sensitivity analysis on ϕ_o. This study consists on randomly perturb all the parameters of ϕ_o by taking uniform variations in a range of $[-\alpha\%, +\alpha\%]$ of their value. This perturbation process is repeated 100 times. For each perturbed mixer, denoted by $\phi_{p,\alpha}$ with $p = 1, ..., 100$, we compute $J_{3D}(\phi_{p,\alpha})$ and compare it to $J_{3D}(\phi_o)$ through the relation:

$$100\frac{|J_{3D}(\phi_o) - J_{3D}(\phi_{p,\alpha})|}{J_{3D}(\phi_o)}. \tag{9}$$

Then, we compute the mean, minimum and maximum values of the Equation (9) regarding the 100 perturbed mixers. The objective of the sensitivity analysis is twofold. On the one hand, we want to know if ϕ_o is close to a local minimum of the design problem when considering the 3D model. To this aim, we apply small perturbations of amplitude $\alpha = 1\%$ and focus on the mixers with lower mixing time than ϕ_o. On the other hand, we want to analyze the robustness of ϕ_o (i.e., the variations on its mixing time) when the parameters are strongly perturbed. For this case, perturbations of amplitude $\alpha = 5\%$, 10% and 20% are taking into account [11].

4   Numerical Results

Here, we present the results obtained by performing the experiments described in Section 3 when considering the denaturant introduced in Section 4.1. In particular, Section 4.2 studies the comparison between the 2D and 3D models, and Section 4.3 analyzes the behavior of the optimized mixer.

4.1   Considered denaturant

During this work, we have considered guanidine hydrochloride (GdCl) as the denaturant [10]. Indeed, GdCl is a Chaotropic agent which is frequently used for protein folding.

The thermophysical variables of GdCl can be approximated as those of water. More precisely, its density is $\rho = 1010$ kg m^{-3} and its dynamic viscosity is $\eta = 9.8 \times 10^{-4}$ kg m^{-1} s^{-1}. Furthermore, the diffusion coefficient of GdCl in the background buffer (assumed to be similar to water) is $D = 2 \times 10^{-9}$ m^2 s^{-1}. According to those coefficients and the restriction $Re = \rho v L/\eta \leq 15$ introduced in Section 2.2, the maximum side injection velocity is $u_s \leq 7$ m s^{-1}.

Finally, the values of α and ω in Equation (4) adapted to GdCl are considered here as 0.9 and 0.3, respectively [11, 14].

4.2   Comparison between the 2D and 3D models

In Table 1, we report the mean, minimum and maximum relative percent variation values between the solutions of Equations (5)-(7) obtained by the 2D and 3D models. The mean percent variation in the mixing time is 15.3%, showing that the 2D model approximates, in a reasonable way, the mixing time predicted by the 3D model. As can be seen, the largest percent variations are obtained in the velocity field, with a mean percent variation of 18.7% versus only 9.8% for the concentration distributions. From these results, we may conclude that the ability of the 2D model to match the solutions (e.g., mixing time or concentrations) of the 3D model is sufficient.

Table 1: Mean, minimum and maximum percent variation (%) of the mixing time, concentration distribution in the plane $z = 0$ μm and velocity field in the plane $z = 0$ μm obtained when considering the 100 microfluidic mixers randomly generated during the 2D-3D comparison experiments detailed in Section 3.2.

	Mean	Minimum	Maximum
Mixing time	15.3	1.2	56.7
Concentration	9.8	0.2	18.7
Velocity field	18.7	3.4	32.9

An important feature of the 2D model is its ability to preserve the same order of mixing time between two different mixer designs as the 3D model (i.e., if $J_{2D}(\phi_1) \leq J_{2D}(\phi_2)$ then $J_{3D}(\phi_1) \leq J_{3D}(\phi_2)$, for most of ϕ_1 and $\phi_2 \in \Phi$). For this purpose, we represent in Figure 3 the 2D mixing time of the 100 mixers generated previously, sorted according to their 2D mixing time, as well as their respective 3D mixing times. The 3D mixing time order is preserved in 72% of the cases. In addition, when the order between two consecutive mixers is not conserved, the difference in their mixing times is, on average, about 12% which can be considered as a low value.

All these results suggest that the optimization process can be performed by using the 2D model instead of the 3D one.

4.3 Analysis of the optimized mixer

The optimization problem (8) has been solved by considering the 2D model and the MSA method presented in Section 3.3 with $(l_{\max}, N_g, N_p, p_m, p_c) = (20, 20, 20, 0.5, 0.55)$. This set of MSA parameters has given good results (in terms of computational time and precision) on other complex optimization problems [30, 31, 33]. The convergence history of the MSA is depicted in Figure 4. The number of evaluations of J_{2D} used by MSA was about 6000 and the optimization process spent around 60 h. Notice that, as a single evaluation of J_{3D} takes approximatively 30 min, solving the same optimization problem with the 3D model could require more than 125 days, which is not a reasonable time.

The values of ϕ_o are reported on Table 2. The shape of the optimized microfluidic mixer, its concentration distribution and the concentration evolution of a particle in its central streamline, obtained with the 2D model, are depicted in Figure 5. The maximum side injection velocity is $u_s =$5.2 m s^{-1}, whereas the maximum central injection velocity is $u_c =$0.038 m s^{-1}. The Reynolds number Re, defined in Section 2.2, is around 9. The mixing time associated to this mixer is about 0.10 μs. This value is 10 times lower than the mixing times achieved by previous mixer designs with the same 2D model [11, 12, 14]. In those works, the mixing times were each greater than
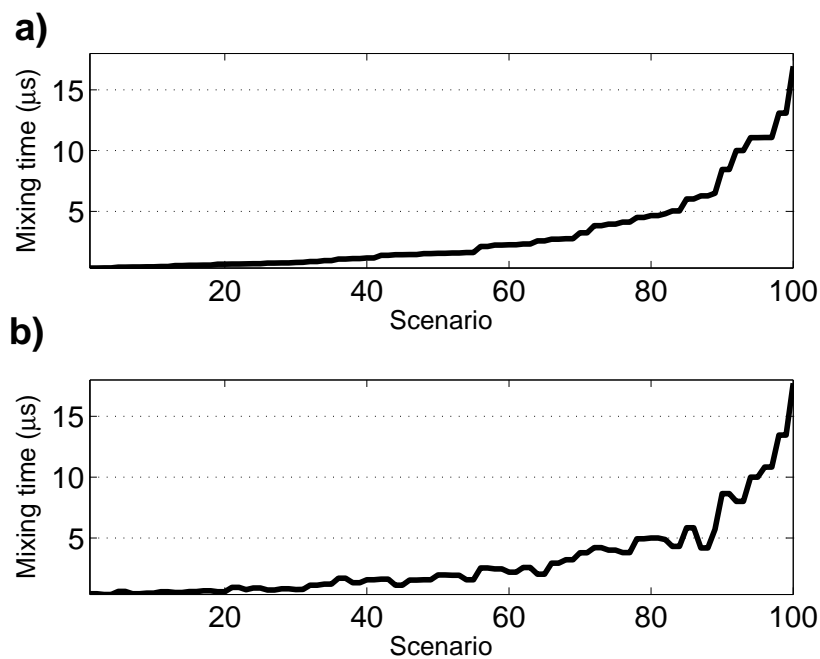
Figure 3: Mixing times of the 100 microfluidic mixers (called Scenarios), randomly generated during the 2D versus 3D comparison process and sorted considering the 2D mixing time, as computed when considering **a)** the 2D model and **b)** the 3D model.
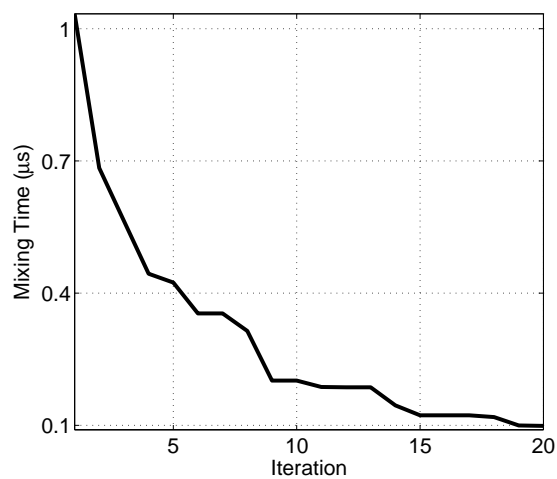

Figure 4: Convergence history of the MSA obtained during the optimization process.

Table 2: Values of the optimized microfluidic mixer parameters presented in Section 4.3.

Parameter	u_s	p	θ	l_c	l_s	l_e	cx_1
Value	5.2	7.3×10^{-3}	0.6	2.5	9.1	16.3	1.1

Parameter	cy_1	l_1	h_1	cx_2	cy_2	l_2	h_2
Value	16.6	0.5	0.3	0.9	18.9	0.1	1.1
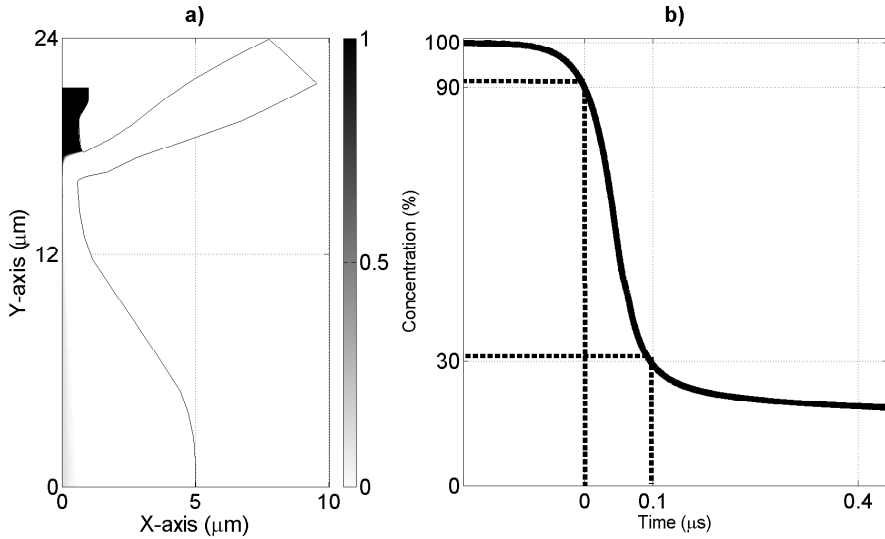
Figure 5: Optimized mixer simulated with the 2D model: **a)** shape of the optimized mixer with a superposed color plot of the denaturant concentration distribution and **b)** the time evolution of the denaturant concentration of a particle in the symmetry streamline.

1 μ. We attribute this improvement mainly to three factors: (i) the angle θ of the inlet side channels, whose value is about $\pi/5$ radians (this angle was fixed to 0 in [11, 12, 14]); (ii) the width of the mixing region (i.e., the area, defined by $(x, y) \in [0, 2] \times [14, 19]\mu$m and depicted in Figure 6, where both fluids are mainly mixed) which reaches a minimum value of about 1.1 μm; and (iii) the choice of adequate injection velocities. Indeed, as can be observed in Figure 6, the shape of both corners Γ_{w1} (stretched along the Y-direction) and Γ_{w2} (sharply pointed wedge pointing roughly along the Y-axis) yields a reduced channel width of 1.1 μm near y = 16.5 μm, where the maximum velocity rises up to 26 m s^{-1}, which helps to accelerate the mixing time. Moreover, we note that the optimized value of θ is consistent with the experimental work described in [13]. Such a study highlights the importance of inclined side channels to prevent strong centripetal accelerations in the inlet side channel streams, which deteriorate the mixer performances.
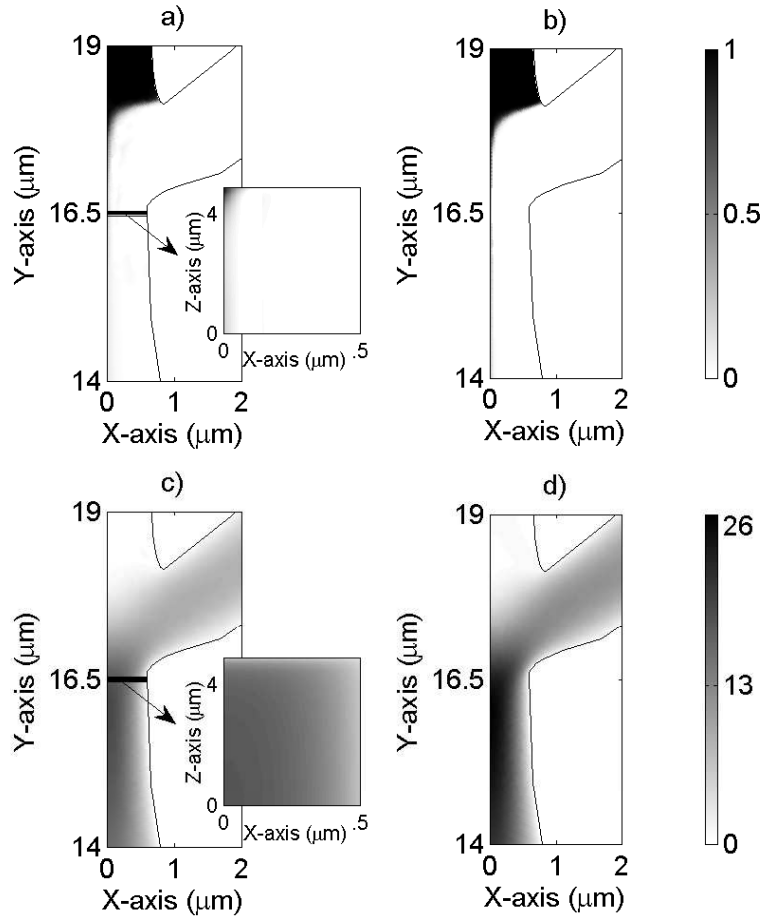
16

Figure 6: Comparison of the solutions obtained in the mixing region with the optimized mixer considering the 3D model (subfigures **a)** and **c)**) and the 2D model (subfigures **b)** and **d)**). **a)** and **b)** show denaturant concentration distributions while **c)** and **d)** plot velocity amplitude distributions in the symmetric plane $z = 0$ μm. For the 3D case, the figure also shows, in the inset detail views, the X-Z plane slices of the concentration and velocity amplitude distributions at the plane defined by y=16.5μm (represented with a horizontal black lines).

Table 3: Mean, minimum and maximum percent variation (%) in the mixing time obtained by considering the 3D model and by perturbing randomly all the parameters of ϕ_o with a maximum amplitude of $1\%, 5\%, 10\%$ and 20% of their initial value.

Maximum Amplitude	Mean	Minimum	Maximum
1%	1.2	0.1	2.1
5%	6.1	0.6	12.7
10%	13.7	2.5	29.2
20%	21.7	4.4	45.7

We also compute the mixing time for this optimum design using the 3D model. To this aim, we extrude the 2D optimal shape (see Figure 7) and we evaluate it using the 3D model. The predicted mixing time is also around 0.10 μs (the difference in mixing times with the 2D model is lower than about 4%). In Figure 6, we show the concentration and velocity amplitude distributions achieved by the 2D and 3D models in the $z = 0$ μm midplane and considering the mixing region. Both solutions exhibit similar characteristics, although we can observe some differences, especially in the velocity field; for the 3D case: (i) Re is around 7 (instead of 9 in te 2D case); and (ii) the maximum velocity reached near y = 16.5 μm is 19 m s^{-1} (instead of 26 m s^{-1} in te 2D case). Figure 7-**a)** shows selected streamlines generated by the 3D velocity field. As we can observe on this figure, the fluid remains laminar. The concentration distribution as well as the velocity amplitude distribution, both obtained with the 3D model, are shown in Figure 7-**b)** and -**c)**, respectively. These two figures exhibit the so-called wall effect [34], since the no-slip condition at the mixer walls results in low velocity values near those walls. This can also be observed in Figure 6, where the X-Z slices of the concentration and velocity amplitude distributions are depicted. These low velocities result in higher denaturant concentrations in these regions. However, the mixer is designed to be relatively insensitive to such wall effects by maintaining a relatively large depth of 10 μm (while having a minimum channel width of 1.1 μm in the mixing region).

The results of the sensitivity analysis of the optimized parameters presented in Section 3.4 when $\alpha = 1\%, 5\%, 10\%$ and 20% are reported on Table 3.

We first focus on the case where the amplitude of the perturbations applied to ϕ_o are lower than 1%. We observe that the optimized mixer has a better mixing time in 77% of the cases. We attribute the imperfect prediction of the 3D optimum to, on the one hand, the lack of precision of the considered MSA method (due to the high computational time required to evaluate Equation (4), the number of iteration of the algorithm, and thus its precision, has been restricted) and, on the other hand, the differences between the 2D and 3D models. However, it is important to mention that
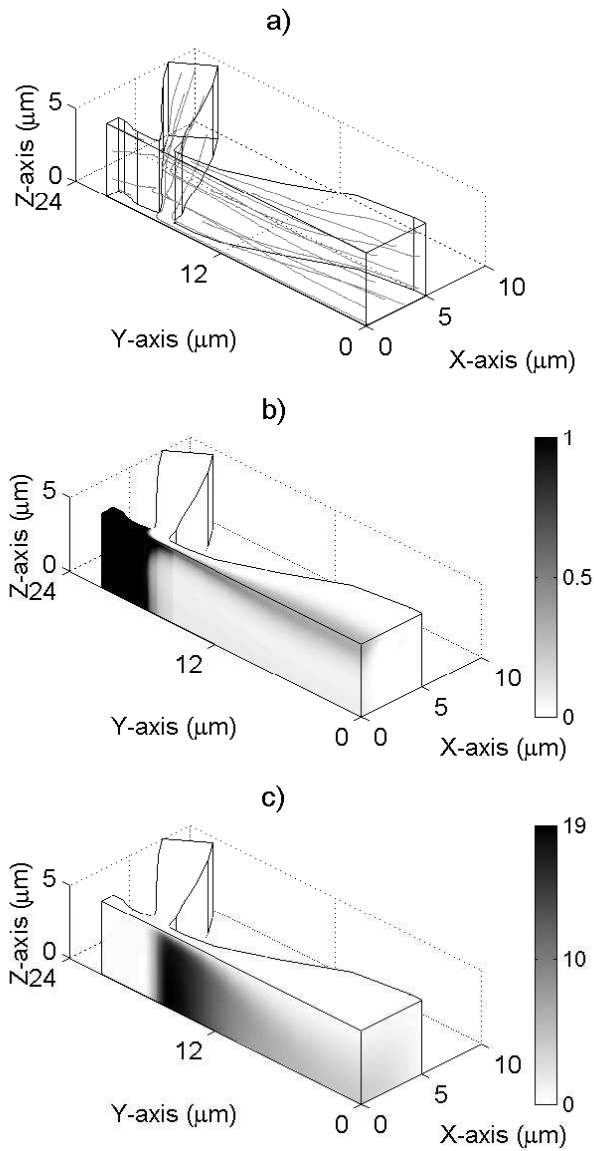
Figure 7: Sample results from the optimized mixer design as simulated with the 3D model. Shown are isometric views of the shape of the optimized mixer with representation of **a)** selected streamlines generated by considering the velocity field, **b)** the concentration distribution, and **c)** the velocity amplitude distribution.

the mean mixing time variation between the optimized mixer and the mixers with the lowest mixing times, is smaller than 0.4%. This result suggests that the optimized mixer may be considered a solution close to a local minimum of Problem (8) when the 3D model is used.

Furthermore, as can be seen on Table 3-Column *Mean*, the mean percent variation in the mixing time (caused by variations in the input parameters) is proportional to the maximum percent variation of the parameter perturbation. In particular, the mixing times of the perturbed mixers are of the same order than the mixing time of the optimized mixer, suggesting the optimized solution is stable. Additionally, even in the worst case (i.e., Table 3-Line 20%-Column *Maximum*), the perturbed mixer still exibits a mixing time of 0.15 μs, which is a significant improvement compared to previous mixers proposed in literature [11, 12]. All those results indicate that ϕ_o is a robust solution for our design problem.

5 Conclusions

We have been explored the design of a particular fast hydrodynamic focusing microfluidic mixer for protein folding. The objective was to reduce the mixing time of this kind of mixer by optimizing the shape (in particular the angle of the side channels) and the injection velocities.

To this aim, firstly, we have introduced a mathematical model used to compute the mixing time of a mixer according to the defined design variables. This model has been presented in 2D and 3D versions. Results show that the 2D and 3D models exhibit similar behaviors regarding the mixing time. Thus, we concluded that the 2D model can be used in the optimization process to greatly reduce the computational time.

Secondly, we defined the optimization problem associated to the design of our device, and solved this using a MSA. The optimized mixer shows a mixing time of 0.1 μs, which represented a decrease of a factor 10 compared to previous known mixers.

Finally, we have verified the robustness of the optimized mixer performances when perturbing its optimization parameters.

The next step, which is currently in preparation (*Ivorra B, Redondo J, Santiago JG, Ramos AM, Ortigosa PM. 3d modeling for the sensitivity analysis of an optimized fast hydrodynamic focusing microfluidic mixer for protein folding.*), is to perform a deeper sensitivity analysis, regarding the optimization parameters and other fixed variables (such as the mixer depth), in order to provide better recommendations and guidelines for the device fabrication process.

References

[1] Berg JM, Tymoczko JL, Stryer L. *Biochemistry* (5th edition). New York: W.H. Freeman, 2002.

[2] Roder H. Stepwise helix formation and chain compaction during protein folding. *Proceedings of the National Academy of Sciences of the USA* 2004; **101**: 1793-1794.

[3] Infante JA, Ivorra B, Ramos AM, Rey JM. On the Modeling and Simulation of High Pressure Processes and Inactivation of Enzymes in Food Engineering. *Mathematical Models and Methods in Applied Sciences* 2009; **19**(12): 2203-2229.

[4] Dobson CM. Protein folding and misfolding. *Nature* 2003; **426**: 884-890.

[5] Jones CM, Henry ER, Hu Y, Chan CK, Luck SD, Bhuyan A, Roder H, Hofrichter J, Eaton WA. Fast events in protein folding initiated by nanosecond laser photolysis. *Proceedings of the National Academy of Sciences of the USA* 1993; **90**:11860-11864.

[6] Jacob M, Holtermann G, Perl D, Reinstein J, Schindler T, Geeves MA, Schmid FX. Microsecond folding of the cold shock protein measured by a pressure jump technique. *Biochemistry* 1999; **38**: 2882-2891.

[7] Park SH, Shastry MCR, Roder H. Folding dynamics of the b1 domain of protein g explored by ultrarapid mixing. *Nature, Structural Biology* 1999; **6**: 943-947.

[8] Mansur EA, Mingxing YE, Wang Y, Dai Y. A State-of-the-art review of mixing in microfluidic mixers. *Chinese Journal of Chemical Engineering* 2008; **16**(4): 503-516.

[9] Brody JP, Yager P, Goldstein RE, Austin RH. Biotechnology at low Reynolds numbers. *Biophysical Journal* 1996; **71**(6), 3430-3441.

[10] Dunbar J, Yennawar HP, Banerjee S, Luo J, Farber GK. The effect of denaturants on protein structure. *Protein Science* 1997; **6**(8): 1727-1733.

[11] Hertzog DE, Ivorra B, Mohammadi B, Bakajin O, Santiago JG. Optimization of a Microfluidic Mixer for Studying Protein Folding Kinetics. *Analytical chemistry* 2006; **78**(13): 4299-4306.

[12] Hertzog DE, Michalet X, Jager M, Kong X, Santiago JG, Weiss S, Bakajin O. Femtomole Mixer for Microsecond Kinetic Studies of Protein Folding. *Analytical Chemistry* 2004: **75** (24): 7169-7178.

[13] Yao S, Bakajin O. Improvements in mixing time and mixing uniformity in devices designed for studies of proteins folding kinetics. *Analytical Chemistry* 2007; **79**: 5753-5759.

[14] Ivorra B, Mohammadi B, Santiago JG, Hertzog DE. Semi-deterministic and genetic algorithms for global optimization of microfluidic protein folding devices. *International Journal of Numerical Method in Engineering* 2006; **66**(2): 319-333.

[15] Darnton N, Bakajin O, Huang R, North B, Tegenfeldt J, Cox E, Sturn J, Austin RH. Hydro-dynamics in 2 1/2 dimensions: making jet in a plane. *Journal of Physics: Condensed Matter* 2001; **13**: 4891-4902.

[16] Park HY, Qiu X, Rhoades E, Korlach J, Kwok L, Zipfel WR, Webb AA, Pollack L. Achieving uniform mixing in a microfluidic device: Hydrodynamic focusing prior to mixing. *Analytical Chemistry* 2006; **78**:4465-4473.

[17] Ferreira AJM. *Series: Solid Mechanics and Its Applications.* Springer. MATLAB Codes for Finite Element Analysis **2009; 157**.

[18] Massey B, Ward-Smith J. *Mechanics of Fluids* (8th edn). Taylor & Francis, 2005.

[19] Herold KE, Rasooly A. *Lab-on-a-Chip Technology (Vol. 1): Fabrication and Microfluidics.* Horizonpress, 2009.

[20] Knight JB, Vishwanath A, Brody JP, Austin RH. Hydrodynamic Focusing on a Silicon Chip: Mixing Nanoliters in Microseconds, *Physical Review Letters* 1998; **80**: 3863-3866.

[21] Berger SA, Talbot L, Yao LS. Flow in Curved Pipes. *Annual Review of Fluid Mechanics* 1983; **15**: 461-512.

[22] Dean WR. The streamline motion of fluid in a curved pipe. *Phil. Mag.* 1928; **7**(5): 673-695.

[23] Glowinski R, Neittaanmaki P. *Series: Computational Methods in Applied Sciences.* Springer Partial Differential Equations. Modelling and Numerical Simulation **2008; 16**.

[24] Redondo JL, Fernández J, García I, Ortigosa PM. A robust and efficient global optimization algorithm for planar competitive location problems. *Annals of Operations Research* 2009; **167**: 87-105.

[25] Redondo JL, Fernández J, García I, Ortigosa PM. Solving the Multiple Competitive Location and Design Problem on the Plane. *Evolutionary Computation* 2009; **17(1)**, 21-53.

[26] Redondo JL, Fernández J, García I, Ortigosa PM. Parallel algorithms for continuous competitive location problems. *Optimization Methods & Software* 2008; **23**(5): 779-791.

[27] Goldberg D. *Genetic algorithms in search, optimization and machine learning.* Addison Wesley, 1989.

[28] Debiane L, Ivorra B, B. Mohammadi B, Nicoud F, Ern A, Poinsot T, Pitsch H. A low-complexity global optimization algorithm for temperature and pollution control in flames with complex chemistry. *International Journal of Computational Fluid Dynamics* 2006; **20(2)**:93–98.

[29] Ivorra B, Ramos AM, Mohammadi B. Semideterministic global optimization method: Application to a control problem of the burgers equation. *Journal of Optimization Theory and Applications* 2007; **135**(3): 549-561.

[30] Gomez S, Ivorra B, Ramos AM. Optimization of a pumping ship trajectory to clean oil contamination in the open sea. *Mathematical and Computer Modelling* 2011; **54**(1): 477-489.

[31] Isebe D, Bouchette F, Azerad P, Ivorra B, Mohammadi B. Shape optimization of geotextile tubes for sandy beach protection. *International Journal of Numerical Method in Engineering* 2008; **174(8)**: 1262- 1277.

[32] Ivorra B, Mohammadi B, Dumas L, Durand O, Redont P. Semi–deterministic vs. genetic algorithms for global optimization of multichannel optical filters. *International Journal of Computational Science for Engineering* 2006; **2(3)**, 170-178.

[33] Ivorra B, Mohammadi B, Ramos AM. Optimization strategies in credit portfolio management. *Journal Of Global Optimization* 2009; **43**(2): 415-427.

[34] Ismagilov RF, Stroock AD, Kenis PJA, Whitesidesa G, Stonea HA. Experimental and theoretical scaling laws for transverse diffusive broadening in two-phase laminar flows in microchannels. *Applied Physics letters* 2000; **76**(17): 2376-2378.

PREPUBLICACIONES DEL DEPARTAMENTO
DE MATEMÁTICA APLICADA
UNIVERSIDAD COMPLUTENSE DE MADRID
MA-UCM 2011

1. APPROXIMATING TRAVELLING WAVES BY EQUILIBRIA OF NON LOCAL EQUATIONS, J. M. Arrieta, M. López-Fernández and E. Zuazua.

2. INFINITELY MANY STABILITY SWITCHES IN A PROBLEM WITH SUBLINEAR OSCILLATORY BOUNDARY CONDITIONS, A. Castro and R. Pardo

3. THIN DOMAINS WITH EXTREMELY HIGH OSCILLATORY BOUNDARIES, J́. M. Arrieta and M. C. Pereira

4. FROM NEWTON EQUATION TO FRACTIONAL DIFFUSION AND WAVE EQUATIONS, L. Váquez

5. EL CÁLCULO FRACCIONARIO COMO INSTRUMENTO DE MODELIZACIÓN, L. Váquez and M. P. Velasco

6. THE TANGENTIAL VARIATION OF A LOCALIZED FLUX-TYPE EIGENVALUE PROBLEM, R. Pardo, A. L. Pereira and J. C. Sabina de Lis

7. IDENTIFICATION OF A HEAT TRANSFER COEFFICIENT DEPENDING ON PRESSURE AND TEMPERATURE, A. Fraguela, J. A. Infante, Á. M. Ramos and J. M. Rey

8. A NOTE ON THE LIOUVILLE METHOD APPLIED TO ELLIPTIC EVENTUALLY DEGENERATE FULLY NONLINEAR EQUATIONS GOVERNED BY THE PUCCI OPERATORS AND THE KELLER–OSSERMAN CONDITION, G. Díaz

9. RESONANT SOLUTIONS AND TURNING POINTS IN AN ELLIPTIC PROBLEM WITH OSCILLATORY BOUNDARY CONDITIONS, A. Castro and R. Pardo

10. BE-FAST: A SPATIAL MODEL FOR STUDYING CLASSICAL SWINE FEVER VIRUS SPREAD BETWEEN AND WITHIN FARMS. DESCRIPTION AND VALIDATION. B. Ivorra B. Martínez-López, A. M. Ramos and J.M. Sánchez-Vizcaíno.

11. FRACTIONAL HEAT EQUATION AND THE SECOND LAW OF THERMODYNAMICS, L. Vázquez , J. J. Trujillo and M. P. Velasco

12. LINEAR AND SEMILINEAR HIGHER ORDER PARABOLIC EQUATIONS IN R^N, J. Cholewa and A. Rodríguez Bernal

13. DISSIPATIVE MECHANISM OF A SEMILINEAR HIGHER ORDER PARABOLIC EQUATION IN R^N, J. Cholewa and A. Rodríguez Bernal

14. DYNAMIC BOUNDARY CONDITIONS AS A SINGULAR LIMIT OF PARABOLIC PROBLEMS WITH TERMS CONCENTRATING AT THE BOUNDARY, A. Jimémez-Casas and A. Rodríguez Bernal

15. DISEÑO DE UN MODELO ECONÓMICO Y DE PLANES DE CONTROL PARA UNA EPIDEMIA DE PESTE PORCINA CLÁSICA, E. Fernández Carrión, B. Ivorra, A. M. Ramos, B. Martínez-López, Sánchez-Vizcaíno.

16. BIOREACTOR SHAPE OPTIMIZATION. MODELING, SIMULATION, AND SHAPE OPTIMIZATION OF A SIMPLE BIOREACTOR FOR WATER TREATMENT, J. M. Bello Rivas, B. Ivorra, A. M. Ramos, J. Harmand and A. Rapaport

1. ON THE CAHN-HILLIARD EQUATION IN H^1(R^N), J. Cholewa and A. Rodríguez Bernal

2. GENERALIZED ENTHALPY MODEL OF A HIGH PRESSURE   SHIFT FREEZING PROCESS, N. A. S. Smith, S. S. L. Peppin and A. M. Ramos

3. 2D AND 3D MODELING AND OPTIMIZATION FOR THE DESIGN OF A FAST HYDRODYNAMIC FOCUSING MICROFLUIDIC MIXER, B. Ivorra, J. L. Redondo, J. G. Santiago, P.M. Ortigosa and A. M. Ramos